Chemical Science

Accepted Manuscript

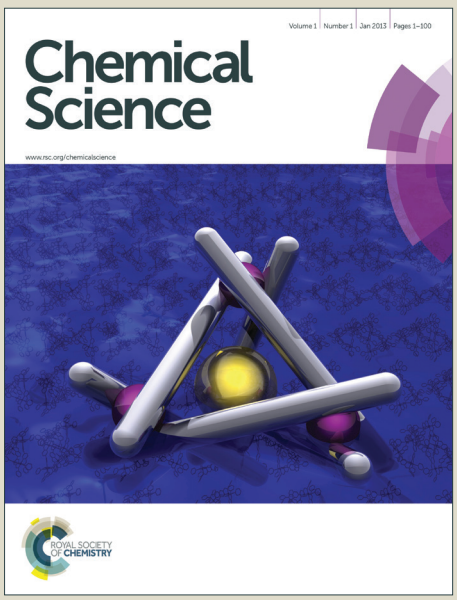

ROYAL SOCIETY OF CHEMISTRY

www.rsc.org/chemicalscience

Journal Name

RSCPublishing

ARTICLE

Metallic Behaviour in Acid Doped Highly Conductive Polymers

Cite this: DOI: 10.1039/x0xx00000x

Nicolas Massonnet,[a] Alexandre Carella,[*,a] Arnaud de Geyer,[b] Jérôme Faure-Vincent,[c] and Jean-Pierre Simonato[*, a]

Received ooth January 2012,
Accepted ooth January 2012

DOI: 10.1039/x0xx00000x

www.rsc.org/

Conductive polymers such as poly(3,4-ethylenedioxythiophene) (PEDOT) meet a wide range of applications as transparent electrodes, hole injecting layers or thermoelectric materials for room-temperature applications. However progress is needed to enhance the electrical conductivities of the materials and to provide understanding about their structure-transport relationships. This work presents the first synthesis of highly conductive PEDOT-based polymers using iron(III)trifluoromethanesulfonate as oxidant. The metallic behaviour of the polymer is revealed by conductivity monitoring from 3 to 300 K. The electrical conductivity is further improved (to 2273 S cm^{-1}) using acids, leading to a positive temperature coefficient of resistivity at an unprecedented 45.5 % oxidation state. X-ray photoemission spectroscopy (XPS) and time of flight - secondary ion mass spectrometry (ToF-SIMS) analyses demonstrate a full replacement of the trifluoromethanesulfonate anions by hydrogen sulphate counter ions. This substitution results in an increased charge carriers' concentration (measured in organic electrochemical transistors), that, together with an enhancement of the mean size of crystalline domains (highlighted by SAXS/WAXS), explain the 80 % increase of electrical conductivity.

Introduction

As one of the most easily processible conductive polymers, poly(3,4-ethylenedioxythiophene) (PEDOT) in combination with poly(styrenesulfonate) (PSS), has focused a lot of scientific interest in the past years.[1] Its electrical conductivity, σ, has been increased by chemical treatments inducing the partial removal of the excess of PSS which acts both as dopant and insulating material.[2–6] On the other hand, a successful route to obtain PEDOT has recently been demonstrated through the polymerization of 3,4-ethylenedioxythiophene (EDOT) using iron(III) para-toluenesulfonate ($Fe(OTs)_3$) as oxidative agent and poly(ethylene glycol)-block-poly(propylene glycol)-block-poly(ethylene glycol) (PEG-PPG-PEG) as surfactant.[7] The low molecular disorder in such PEDOT layers induces a semi-metallic conduction mechanism according to Crispin et al.[8] Taking these reports into account, we considered the possibility to further improve the conductivity of PEDOT materials by using less hindered and poorly coordinating counter anions, which would optimize both the weight fraction and the oxidation level of PEDOT. Accordingly, the present work demonstrates the oxidative chemical polymerization of EDOT using iron(III) trifluoromethanesulfonate ($Fe(OTf)_3$) through a method involving PEG-PPG-PEG. The resulting materials display metallic properties that are even strengthened by doping with specific acids. In particular sulphuric acid enhances σ up to 2273 S cm^{-1} (1.8 fold increase), and induces a positive temperature coefficient of resistivity (TCR). Though this study is focused on PEDOT polymerized with OTf anion (PEDOT:OTf) due to the novelty of this material, it is noteworthy that the doping method performed hereby is also efficient on PEDOT polymerized with OTs anion (PEDOT:OTs).

Results and Discussion

Electrical conductivity and morphology

The optimization of the polymerization conditions (Fig. S1) leads to PEDOT:OTf displaying σ = 1218 S cm^{-1}, whereas the typical electrical conductivity for a spin-coated layer of PEDOT:PSS (used as reference material for morphological and structural discussions in this work) is 1 S cm^{-1}. AFM phase contrast images of the surface of PEDOT:OTf and PEDOT:PSS show that PEDOT:OTf has a granular structure with large homogeneous domains while PEDOT:PSS displays a poorly structured surface where hard and soft domains are highly entangled (Fig. 1). The amorphous structure of PEDOT:PSS derives from the excess of PSS, resulting in the embedding of PEDOT:PSS grains in a PSS-rich matrix. On the contrary, the less sterically hindered OTf ions enable a dense stacking of PEDOT chains resulting in the observed granular structure. The high electrical conductivity of PEDOT:OTf compared with PEDOT:PSS is ascribed to these structural differences, that

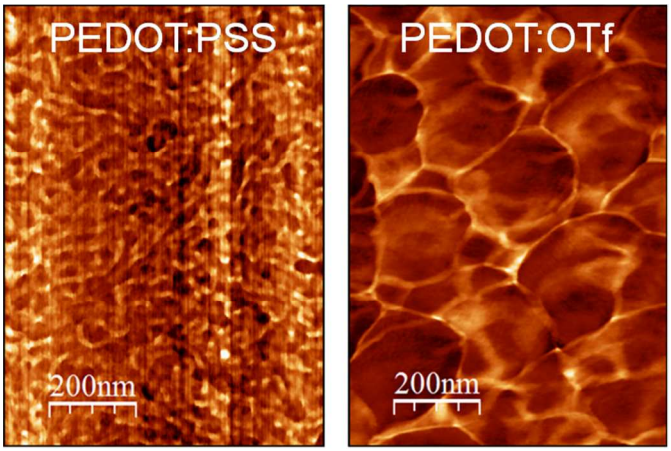

Figure 1: AFM phase images of PEDOT:PSS and PEDOT:OTf

result in a higher fraction of conductive PEDOT in PEDOT:OTf. The influence of various acid solutions on the electrical conductivity of PEDOT:OTf has been tested. Hydrochloric acid (HCl) and nitric acid (HNO_3) induce a downshift of σ to 385 and 740 S cm^{-1}, whereas para-toluenesulfonic (TsOH), trifluoromethanesulfonic (TfOH) and sulphuric (H_2SO_4) acids increase σ respectively up to 1503, 1613 and 2273 S cm^{-1}. The optimum values of σ are obtained at pH ~ 1, whereas when pH is set below 0.5, the treatment results in degradation of the polymer layer.

Ultraviolet-visible-near infrared spectroscopy

The absorbance spectra of PEDOT:OTf layers in its pristine state, and doped with H_2SO_4 and TfOH, are compared with the absorbance spectra of a PEDOT:PSS layer (Fig. 2). The NC absorption band (~ 590 nm) characterizes the π-π* transition in Neutral Chains, the RC absorption band (~ 750 nm) is distinctive of Radical Cations and the large DC absorption band (λ > 1250 nm) reveals the presence of DiCations.[9–12] The strong absorbance in RC and DC bands of PEDOT:OTf suggests a higher density of charge carriers compared with PEDOT:PSS, in accordance with phase imaging data. Upon doping with TfOH or H_2SO_4, the DC band grows wider and its absorbance increases. This observation, together with the increase of σ upon doping, is consistent with the insertion of additional charge carriers in the polymer and an increase of its oxidation level. UV-Vis-NIR data showing the influence of other acids are available in Fig. S2.

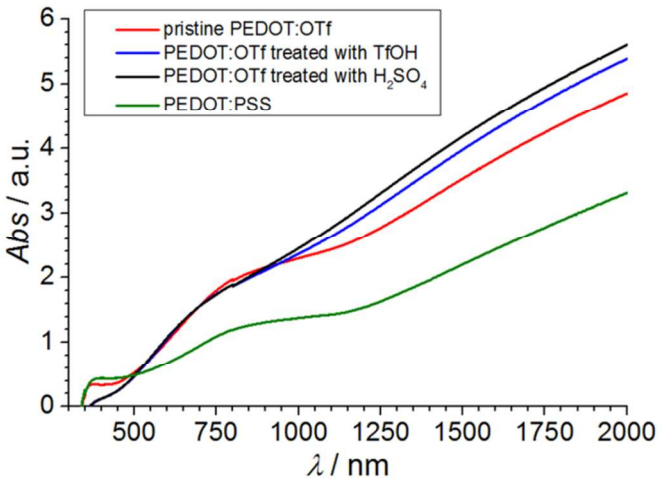

Figure 2: UV-Vis-NIR spectra of PEDOT:OTf in the pristine state, PEDOT:OTf treated with TfOH and PEDOT:OTf treated with H_2SO_4, and PEDOT:PSS

X-ray photoelectron spectroscopy

Layers of PEDOT:OTf, PEDOT:OTf doped with TfOH and PEDOT:OTf doped with H_2SO_4 (hereinafter called PEDOT:Sulf) are analysed by XPS and the resulting overview spectra are presented in Fig. S3. The F(1s) signal (688.5 eV), related to fluorinated species, is a good indicator of the presence of OTf ions inside the layer: the intensity of this signal is slightly increased when PEDOT:OTf is doped with TfOH, supporting the hypothesis that new counter ions are inserted in the polymer. On the other hand, the overview spectra of PEDOT:Sulf has no trace of the F(1s) signal, suggesting that OTf ions have been eliminated from the layer upon doping. The oxidation level of PEDOT layers depends on the ratio of thiophene units to sulphured counter ions, therefore it can be discussed from the disambiguation of the S(2p) signal related to sulfur.[13] For PEDOT:OTf, PEDOT:OTf doped with TfOH and PEDOT:Sulf (Fig. 3), the S(2p) signal clearly reveals peaks from the thiophene units (163-167 eV) and peaks from SO_3^- and HSO_4^- (167-171 eV). The oxidation level calculated from these contributions is 27.8 % for pristine PEDOT:OTf (which is consistent with the oxidation state of pristine PEDOT:OTs reported elsewhere[14]), and it reaches 35.7 % after TfOH doping

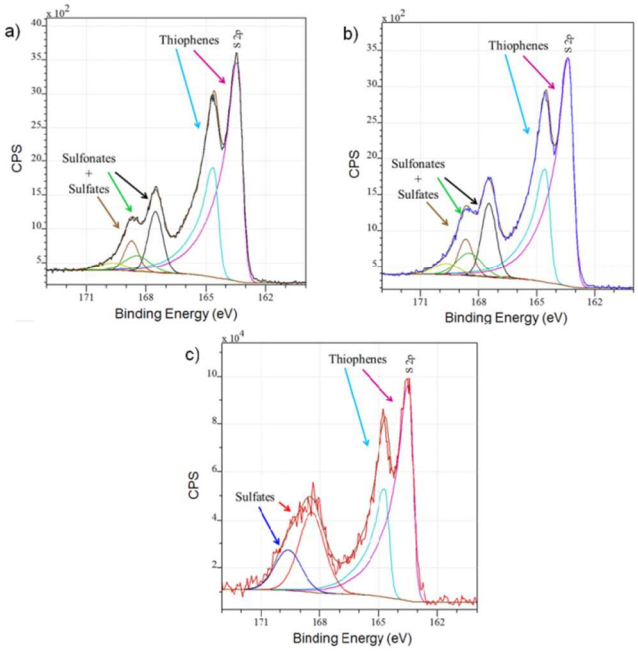

Figure 3: XPS S(2p) signals of a) PEDOT:OTf in the pristine state, b) PEDOT:OTf treated with TfOH and c) PEDOT:Sulf. The disambiguation of the signals is indicated under the experimental curves.

and 45.5 % after H_2SO_4 doping, which is the highest PEDOT oxidation level ever reported to our knowledge. The increase in the oxidation level supports an increase in the charge carriers' concentration. In the case of H_2SO_4 doping, HSO_4^- peaks are the only components of the S(2p) signal in the [167-171 eV] range. This observation strongly suggests that OTf ions have been replaced by HSO_4^- upon doping.

Time of flight-secondary ion mass spectroscopy

XPS analyses are advantageously combined with ToF-SIMS in order to probe the homogeneity of the layer at higher thickness ranges. The intensity profiles versus the sputter depth reported in Fig. 4 are those of the most representative ionic species detected during the analysis. The reported species are $C_6H_5O_2S^-$ ($EDOT^-$, a fragment of PEDOT macromolecules), OTf, CF_3^- (an OTf fragment), and HSO_4^- (either resulting from OTf fragmentation or initially present in the layer). The samples display a homogeneous intensity profile for each ionic species, indicating that the sample composition is uniform regarding the thickness, and confirming that doping reactions take place throughout the whole polymer layer. All the species signals have a similar intensity when comparing PEDOT:OTf in pristine state with PEDOT:OTf doped with TfOH. On the other hand, the intensity profiles measured on PEDOT:OTf and PEDOT:Sulf disclose major differences: OTf and CF_3^- signals are divided respectively by a factor of 154 and 55, whereas HSO_4^- signal is multiplied by 23. These observations support the previously stated doping mechanisms, consisting in the replacement of OTf ions with HSO_4^-, and confirm their occurrence in the entire thickness of the layer.

Small and wide angle X-ray scattering

The SAXS/WAXS intensity profiles of thin PEDOT:PSS, PEDOT:OTf and PEDOT:Sulf films are presented in Fig. 5. In order to facilitate the reader's understanding, a schematic representation of the crystalline structure of PEDOT:OTf (inspired from previous works on PEDOT:OTs[15]) is provided in the figure. PEDOT:PSS intensity profile exhibits two broad humps at $q \sim 0.29$ Å^{-1} ($d = 22$ Å) and 0.46 Å^{-1} ($d = 14$ Å), and two peaks at $q = 1.22$ Å^{-1} ($d = 5.2$ Å) and $q = 1.82$ Å^{-1} ($d = 3.4$ Å). The weak hump centred on 0.29 Å^{-1} is assigned to the lamellar stacking distance [$d(100) = 22$ Å] peak occurring from the alternate ordering of the PEDOT and PSS polymer chains. This distance is in agreement with PEDOT and PSS chains widths (7.5 Å and 15.5 Å, respectively).[16] The narrow peak at $q = 1.82$ Å^{-1} indicates the Bragg reflection from PEDOT oligomers stacking face-to-face along the *b*-axis with a spacing of 3.4 Å in agreement with the π-π stacking distance [d(010)] of the PEDOT thiophenes.[15] From the Scherrer formula[17] applied to the 010 diffraction peak, we calculate a crystalline domain size of ~ 33 Å along the *b*-axis. The other peaks at $q = 0.46$ Å^{-1} and 1.22 Å^{-1} are attributed to the interdigitation packing and π-π stacking distance of PSS.[15–18] Moreover, for $q < 0.2$ Å^{-1}, we observed a $\sim q^{-4}$ power law indicating the contribution from sharply defined interface separating the PEDOT-rich crystalline grains from the PSS-rich amorphous matrix.[19] The intensity profile for PEDOT:OTf and PEDOT:Sulf exhibits several diffraction peaks at $q = 0.45$ Å^{-1} ($d = 14$ Å), 0.89 Å^{-1} ($d = 7.0$ Å), and 1.82 Å^{-1} ($d = 3.4$ Å) corresponding to the (100), (200), and (020) planes of PEDOT.[15] A large shift arises in the lamellar stacking peak position (100) when comparing PEDOT:PSS ($q \sim 0.29$ Å^{-1}) and PEDOT:OTf ($q \sim 0.45$ Å^{-1}). This corresponds respectively to large [$d(100) = 22$ Å] and short [$d(100) = 14$ Å] stacking distances due to the width differences between PSS macromolecules and OTf ions. The low lamellar stacking distance in PEDOT:OTf results in stronger interaction between PEDOT chains which is favourable to an increase of the crystalline order degree. All the distinct diffraction peaks in PEDOT:OTf are larger and sharper than in PEDOT:PSS consistently with a growth of the thickness and number of crystalline domains. The crystallite size along the *b*-axis (L_b), derived from the (020) peak is approximately 37 Å in PEDOT:OTf compared to approximately 33 Å in PEDOT:PSS. The crystallite size (L_a) along the a-axis, derived from the (100) diffraction peak, is approximately 60 Å in PEDOT:OTf film. These observations are in accordance with the structural changes observed with the AFM phase contrast imaging. At small angles ($q < 0.2$ Å^{-1}), the intensity profile follows a q^{-3} dependence. This power law in the SAXS domain highlights the absence of discontinuity in the material. Several changes can be noticed when comparing X-ray patterns of PEDOT:OTf and PEDOT:Sulf. Although the diffraction peaks' intensities remain essentially un-changed, a sharpening is observed in the (100) and (200) peaks. This is consistent with a constant number of crystalline domains before and after H_2SO_4 treatment, together with an increase of their size along the *a*-axis: L_a (calculated from Scherrer formula) is approximately 77 Å in PEDOT:Sulf. At last, a small peak is observed at $q \sim 1.62$ Å^{-1}, corresponding to a distance ~ 3.9 Å, which is comparable to the periodicity of monomer units of PEDOT (~ 3.85 Å).[15] The effects on the structural order along the *a*-axis may be

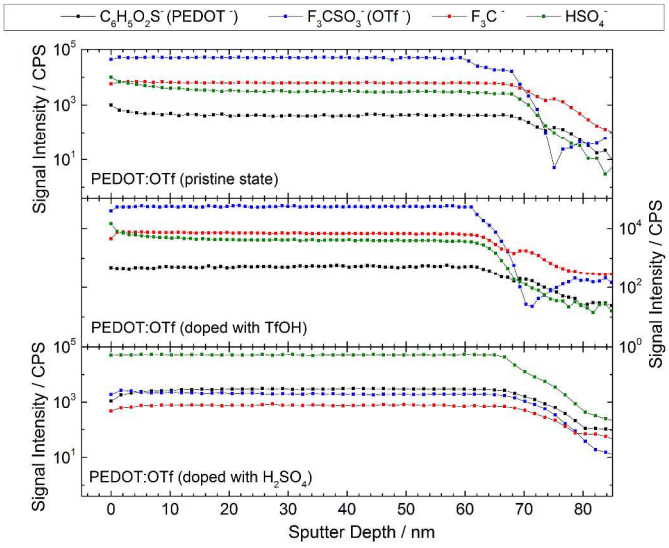

Figure 4: ToF-SIMS intensity profiles of different ionic species in ~65nm thick layers of PEDOT:OTf in pristine state, PEDOT:OTf treated with TfOH and PEDOT:Sulf

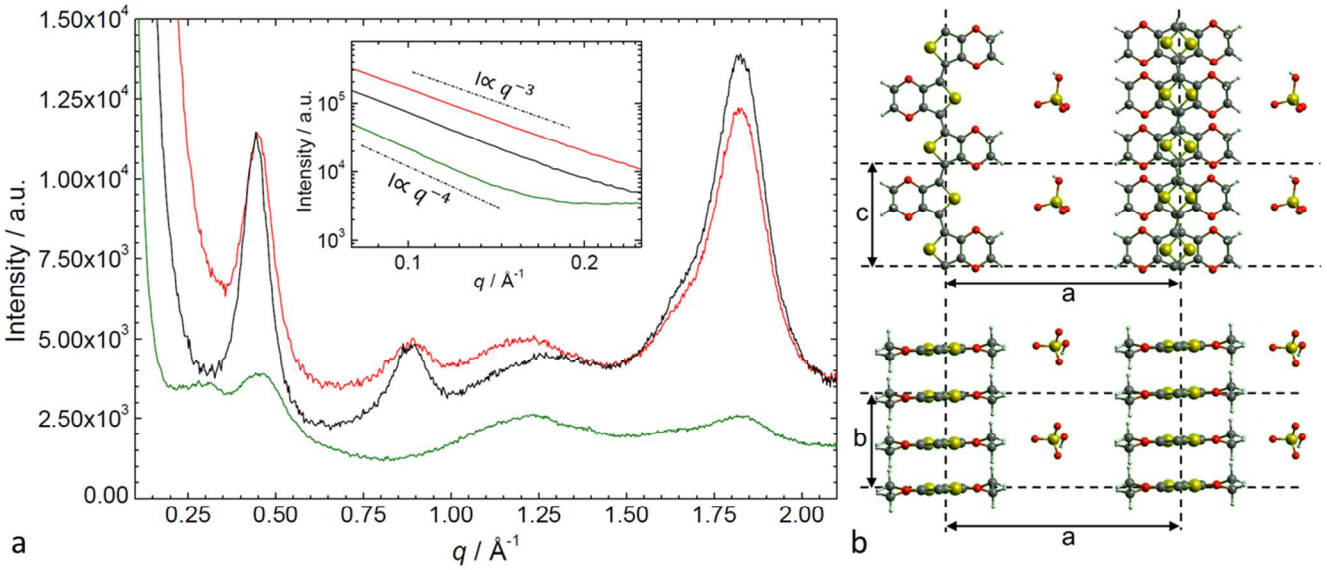

Figure 5: a) SAXS/WAXS intensity profile of PEDOT:PSS (green line), PEDOT:OTf in the pristine state (red line) and PEDOT:Sulf (black line). Top inset shows the intensity in the small angles domain. b) Schematic illustration of the structural model of PEDOT:OTf, in projections along the *b*-axis (upper) and the *c*-axis (lower) directions. This illustration is adapted from reference [15] and is provided as a support for the discussion

attributed to the inserted ions implying less steric hindrance than OTf anions, thus inducing more crystalline order at longer distances. This capacity of HSO_4^- to enable more linear PEDOT structures is supported by the observation of a small peak at $q \sim 1.62$ Å^{-1}, matching the periodicity of the monomer unit. Consistently with this interpretation, this tiny peak was not observed on the intensity profile of the pristine PEDOT:OTf sample.

Charge carriers concentration

The charge carriers' mobility in PEDOT:PSS, PEDOT:OTf and PEDOT:Sulf is evaluated with an Organic ElectroChemical Transistor (OECT) as described by Ishida et al. for PEDOT:PSS.[20] Apparatus description and output curves are available in Fig. S4 and S5. The charge carriers' concentration is calculated from the values of the mobility and σ, measured on thin polymer films. The electronic mobility in PEDOT:PSS, PEDOT:OTf and PEDOT:Sulf are respectively 1.3, 0.1 and 0.1 cm^2.V^{-1}.s^{-1}. The high mobility in PEDOT:PSS matches the expectations regarding the quality of polymer chains in commercial formulations. The charge carriers' concentrations of PEDOT:PSS, PEDOT:OTf and PEDOT:Sulf are respectively 1.1×10^{21}, 5.7×10^{22} and 1.6×10^{23} cm^{-3}. Thus the value of σ in PEDOT:OTf is linked to the high charge carriers' concentration ascribed to the PEDOT weight fraction. The increase of the charge carriers' concentration in PEDOT:Sulf compared with PEDOT:OTf is consistent with the oxidation levels deduced from the XPS data.

Transport properties

The variation of σ as a function of temperature, *T*, from 3 to 300 K is plotted in Fig. 6. It provides understanding of the transport mechanisms in PEDOT:PSS, PEDOT:OTf and PEDOT:Sulf. For the PEDOT:PSS sample, σ ~ 1 S cm^{-1} at room temperature, then it collapses over several orders of magnitude at low temperatures, resulting in an extrapolated σ = 0 S cm^{-1} at $T = 0$ K (which is typical for semiconductors). The reduced activation energy, defined as $W=(\mathrm{d}[\ln(\sigma)])/(\mathrm{d}[\ln(T)])$[21] is plotted in the top inset of Fig. 6. For PEDOT:PSS the decrease of *W* with *T* and the ratio σ(300 K)/σ(3 K) > 21000 indicate that the sample is far in the insulating regime. The transport mechanism in PEDOT:PSS fits the VRH model[22] consistently with previous studies[16] and with the embedded structure deduced from our structural observations. For PEDOT:OTf, σ is 1000 S cm^{-1} at room temperature and the ratio σ(300 K)/σ(3 K) equals 1.7, indicating a highly ordered polymer[21] as previously stated (Fig. 1 and 3). From 3 to 45 K, *W* increases with *T*: this is typical of conducting polymers in the metallic side of the Metal-Insulator (M-I) transition.[23] *W* has a constant value of 0.19 from 45 to 149 K and therefore $\sigma \propto T^{0.19}$, which is characteristic of the critical regime.[21] The exponent of the power is less than 1/3, confirming that this sample is in the metallic side of the M-I transition.[23] As a result, VRH conduction regime does not apply and the transport is governed by a power law, accordingly to the continuity of the material and the density of PEDOT chains stacking. The doping of PEDOT:OTf with H_2SO_4 results in an increase of σ (about 40 % at 300 K for this sample). For $T > 5.5$ K, *W* has a positive slope with increasing *T*, placing PEDOT:Sulf in the metallic side of the M-I transition. The slope of *W* is steeper than the one of pristine PEDOT:OTf, and the plateau is replaced by a slight slope. Moreover, σ reaches a minimum at 5.5 K, then slightly increases from 5.5 K to 3 K (Fig. 6 bottom inset). This means that the TCR is positive in this range. The thermopower values of PEDOT:PSS, PEDOT:OTf and PEDOT:Sulf respectively 19, 17 and 14 μV

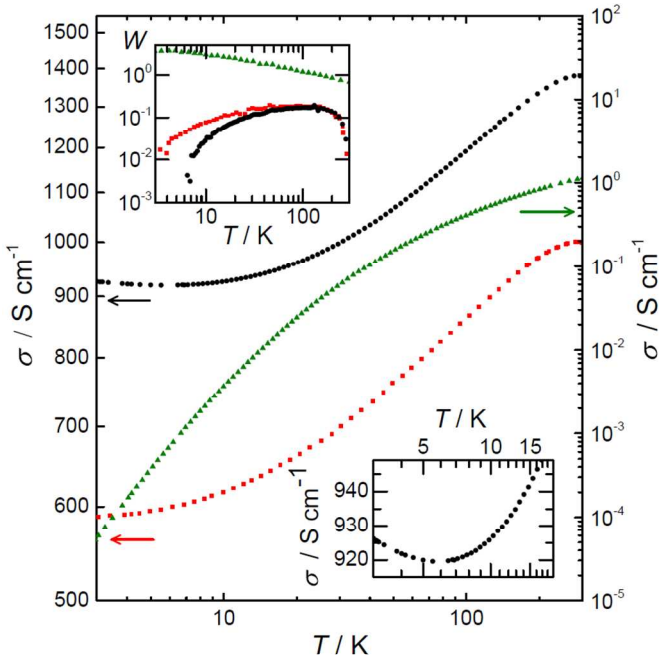

Figure 6: log-log plot of σ as a function of temperature from 3 to 300 K. Left Y axis: PEDOT:OTf (red squares) and PEDOT:Sulf (black circles); right Y axis: PEDOT:PSS (green triangles). Top inset: the corresponding activation energy *W* in a log-log plot. For PEDOT:Sulf, W is negative in the [3 K; 5.5 K] range, as expected for metallic behaviour. Bottom inset: zoom on the electrical conductivity of PEDOT:Sulf in the [3 K; 20 K] *T* range

K^{-1} confirm the stronger metallic behaviour in PEDOT:OTf and PEDOT:Sulf. These values are lower than those observed by Crispin et al. for semi-metallic PEDOT:OTs (55 μV K^{-1})[8] and Pipe et al. for EG-dipped PEDOT:PSS (70 μV K^{-1}).[5] The mobility and structure of PEDOT:OTf and PEDOT:Sulf being similar, the strengthened metallic behaviour (*i.e.* pushing toward the metallic side of the M-I transition) is mainly attributed to the increased charge carriers' concentration (from 5.7×10^{22} to 1.6×10^{23} cm^{-3}) induced by the insertion of HSO_4^-. The positive TCR observed for PEDOT:Sulf is the signature of a "true" metallic behaviour. It is remarkable that, since the discovery of conducting polymers in 1977, very few examples of metallic behaviours (*i.e.* with positive TCR) have been observed in polymer films: PF_6-doped polypyrroles[24], and CSA-doped polyaniline.[23,25,26] The origin of such behaviour is still under debate, related discussions are available in previous reports[27,28] and references therein.

Conclusions

In conclusion, $Fe(OTf)_3$ was used as oxidant for the polymerization of EDOT, resulting in a highly conductive metallic-like PEDOT:OTf polymer presenting an ordered crystalline structure. The treatment of PEDOT:OTf with H_2SO_4 increases the conductivity up to 2273 S cm^{-1} and strengthens the metallic behaviour, whereas the crystalline structure remains mostly unchanged. The oxidation level of the doped polymer (45.5 %) is the highest ever reported for PEDOT, and the dependence of σ towards temperature reveals a positive TCR, disclosing this polymer as one of the very few organic materials demonstrating a metallic behaviour.

Experimental

Chemicals

PEDOT:PSS Clevios PH1000 was purchased from H.C. Starck. P(VDF-HFP), PEG-PPG-PEG (various Mn), acids, EDOT and ethylene glycol (EG) were purchased from Aldrich and used without further purification.

Polymer films preparation

Glass substrates (Corning Eagle XG, 2.5 cm x 2.5 cm, 1.1 mm thick) are washed with acetone and ethanol. A solution of 20 % wt. PEG-PPG-PEG (Mn = 5800 $g.mol^{-1}$) and 80 % wt. ethanol is stirred in an ultrasonic bath for 4 h. $Fe(OTf)_3$ (0.25 $mol.L^{-1}$) is added and the solution is then stirred for 2 h and chilled at 5 °C. EDOT (0.18 $mol.L^{-1}$) is added to the solution. After 1 min stirring in an ultrasonic bath the reaction mixture is spin-coated onto the glass substrates and annealed for 10 min at 70 °C. The resulting layers are washed in ethanol and dried. PEDOT:PSS samples, spin-coated from a dilution of PEDOT:PSS Clevios PH1000 in isopropyl alcohol (20 % wt.), are used as references. Further experimental details are provided in the SI.

Doping treatment

All the acids are diluted in water in order to obtain solutions at pH 0.5. The samples are dipped in the acid solution for 1 h then dried at 160 °C. Experimental conditions are discussed in the SI.

Characterisations

Charge carrier measurements are performed as described by Wei et al. in an OECT[20] using a described ionic gel.[29] σ is monitored from 3 to 300 K using a He flow cryostat Oxford Instruments CF 1200 D. Temperature is measured using a RhFe calibrated resistor and σ is obtained after temperature stabilization at the mK range using the four-probes in line configuration. X-ray patterns measurements samples are fabricated using thin polymer films described hereinbefore. The films are dipped in ethanol then aggregated and dried in order to obtain a ~ 0.5 mm thick polymer block. X-ray patterns were measured in transmission geometry using a home-made SAXS/WAXS camera utilizing a point source (source size ~ 100 μm x 100 μm) Bruker-Nonius (FR591) rotating anode generator, with Cu-Kα radiation (λ = 1.5418 Å) at 45 kV and 26 mA. The samples were freely suspended in the X-ray beam and a multi-wire gas filled large area detector placed at a distance of 20 cm recorded the patterns. Further details are available in the SI. The thermopower *S* is recorded with a ULVAC ZEM-3 system. The thicknesses of the layers and their morphologies are measured by AFM (Bruker Innova). UV-Vis-NIR spectra are recorded on a Varian Cary 5000. XPS are performed on NOVA-KRATOS with an Al K_α monochromatic source. ToF-SIMS is performed with a 5 keV Ar_2^{500+} sputter

gun and a 15 keV Bi^{3+} liquid metal ion gun for the analysis, while the detector is set to negative ion mode.

Notes and references

[a] Univ. Grenoble Alpes, F-38000 Grenoble, France
CEA, LITEN, MINATEC Campus, F-38054 Grenoble, France
[b] Univ. Grenoble Alpes, INAC-SP2M, F-38000 Grenoble, France
CEA, INAC-SP2M, F-38000 Grenoble, France
[c] Univ. Grenoble Alpes, INAC-SPRAM, F-38000 Grenoble, France
CNRS, INAC-SPRAM, F-38000 Grenoble, France
CEA, INAC-SPRAM, F-38000 Grenoble, France
*Corresponding authors :
alexandre.carella@cea.fr; jean-pierre.simonato@cea.fr

Electronic Supplementary Information (ESI) available: Experimental details for polymer synthesis, SAXS/WAXS, charge carriers' mobility and $\sigma(T)$ measurements, supplementary UV-Vis-NIR spectra, XPS overview spectra. See DOI: 10.1039/b000000x/

1. F. Louwet, *Synth. Met.*, 2003, **135-136**, 115–117.

2. Y. Xia, K. Sun, and J. Ouyang, *Adv. Mater.*, 2012, **24**, 2436–40.

3. T.-H. Meen, K.-L. Chen, Y.-H. Chen, W.-R. Chen, D.-W. Chou, W.-H. Lan, and C.-J. Huang, *Int. J. Photoenergy*, 2013, **2013**, 1–6.

4. J. Ouyang, *Displays*, 2013, **34**, 423–436.

5. G.-H. Kim, L. Shao, K. Zhang, and K. P. Pipe, *Nat. Mater.*, 2013, **12**, 719–23.

6. N. Kim, S. Kee, S. H. Lee, B. H. Lee, Y. H. Kahng, Y.-R. Jo, B.-J. Kim, and K. Lee, *Adv. Mater.*, 2014, **26**, 2268–72, 2109.

7. M. V. Fabretto, D. R. Evans, M. Mueller, K. Zuber, P. Hojati-Talemi, R. D. Short, G. G. Wallace, and P. J. Murphy, *Chem. Mater.*, 2012, **24**, 3998–4003.

8. O. Bubnova, Z. U. Khan, H. Wang, S. Braun, D. R. Evans, M. Fabretto, P. Hojati-Talemi, D. Dagnelund, J.-B. Arlin, Y. H. Geerts, S. Desbief, D. W. Breiby, J. W. Andreasen, R. Lazzaroni, W. M. Chen, I. Zozoulenko, M. Fahlman, P. J. Murphy, M. Berggren, and X. Crispin, *Nat. Mater.*, 2013, **13**, 1–5.

9. O. Bubnova and X. Crispin, *Energy Environ. Sci.*, 2012, **5**, 9345.

10. S. Garreau, J. L. Duvail, and G. Louarn, *Synth. Met.*, 2001, **125**, 325–329.

11. M. Łapkowski and A. Proń, *Synth. Met.*, 2000, **110**, 79–83.

12. N. Massonnet, A. Carella, O. Jaudouin, P. Rannou, G. Laval, C. Celle, and J.-P. Simonato, *J. Mater. Chem. C*, 2014, **2**, 1278.

13. X. Crispin, S. Marciniak, W. Osikowicz, G. Zotti, A. W. D. van der Gon, F. Louwet, M. Fahlman, L. Groenendaal, F. De Schryver, and W. R. Salaneck, *J. Polym. Sci. Part B Polym. Phys.*, 2003, **41**, 2561–2583.

14. M. Fabretto, K. Zuber, C. Hall, P. Murphy, and H. J. Griesser, *J. Mater. Chem.*, 2009, **19**, 7871.

15. K. E. Aasmundtveit, E. J. Samuelsen, L. A. A. Pettersson, O. Inganäs, T. Johansson, and R. Feidenhans'l, *Synth. Met.*, 1999, **101**, 561–564.

16. N. Kim, B. H. Lee, D. Choi, G. Kim, H. Kim, J.-R. Kim, J. Lee, Y. H. Kahng, and K. Lee, *Phys. Rev. Lett.*, 2012, **109**, 106405.

17. R. W. James, *Optical Principles of the Diffraction of X-Rays*, Woodbridge, Ox Bow Pre., 1982.

18. T. H. Lee, K. Do, Y. W. Lee, S. S. Jeon, C. Kim, J. Ko, and S. S. Im, *J. Mater. Chem.*, 2012, **22**, 21624.

19. O. Glatter and O. Kratky, *Small Angle X-Ray Scattering*, New York, Academic P., 1982.

20. Q. Wei, M. Mukaida, Y. Naitoh, and T. Ishida, *Adv. Mater.*, 2013, **25**, 2831–6.

21. R. Menon, in *Handbook of Organic Conductive Molecules and Polymers, vol. 4*, ed. H. S. Nalwa, Wiley, 1997, p. 3334.

22. N. F. Mott and E. A. Davis, *Electronic Processes in Non-Crystalline Materials*, New York, Oxford., 1979.

23. R. Menon, C. Yoon, D. Moses, A. Heeger, and Y. Cao, *Phys. Rev. B*, 1993, **48**, 17685–17694.

24. T. Ishiguro, H. Kaneko, Y. Nogami, H. Ishimoto, H. Nishiyama, J. Tsukamoto, A. Takahashi, M. Yamaura, T. Hagiwara, and K. Sato, *Phys. Rev. Lett.*, 1992, **69**, 660–663.

25. K. Lee, S. Cho, S. H. Park, a J. Heeger, C.-W. Lee, and S.-H. Lee, *Nature*, 2006, **441**, 65–8.

26. A. J. Heeger, *Condens. Coherence Condens. Matter - Proc. Nobel Jubil. Symp.*, 2003, 30–35.

27. A. B. Kaiser, *Reports Prog. Phys.*, 2001, **64**, 1–49.

28. A. J. Epstein, in *Handbook of Conducting Polymers*, eds. T. A. Skotheim and J. R. Reynolds, CRC Press, 2007, p. 1680.

29. K. H. Lee, M. S. Kang, S. Zhang, Y. Gu, T. P. Lodge, and C. D. Frisbie, *Adv. Mater.*, 2012, **24**, 4457–62.

